Physical Characterization of the Potentially-Hazardous High-Albedo Asteroid (33342) 1998 WT from Thermal-Infrared Observations

Alan W. Harris, Michael Mueller, Marco Delbó, Schelte J. Bus

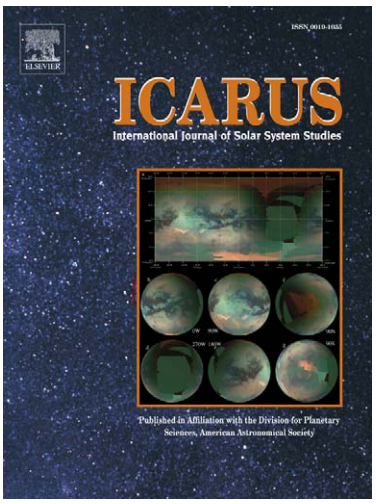

Physical Characterization of the Potentially-Hazardous High-Albedo Asteroid (33342) 1998 WT_{24} from Thermal-Infrared Observations

Alan W. Harris, Michael Mueller, Marco Delbó, Schelte J. Bus

PII: S0019-1035(06)00446-5
DOI: 10.1016/j.icarus.2006.12.003
Reference: YICAR 8146

To appear in: *Icarus*

Received date: 27 September 2006
Revised date: 6 December 2006
Accepted date: 8 December 2006

Please cite this article as: A.W. Harris, M. Mueller, M. Delbó, S.J. Bus, Physical Characterization of the Potentially-Hazardous High-Albedo Asteroid (33342) 1998 WT_{24} from Thermal-Infrared Observations, *Icarus* (2006), doi: 10.1016/j.icarus.2006.12.003

Physical Characterization of the Potentially-Hazardous High-Albedo Asteroid (33342) 1998 WT_{24} from Thermal-Infrared Observations[1]

Alan W. Harris

DLR Institute of Planetary Research, Rutherfordstrasse 2, 12489 Berlin, Germany
E-mail: alan.harris@dlr.de

Michael Mueller

DLR Institute of Planetary Research, Rutherfordstrasse 2, 12489 Berlin, Germany

Marco Delbó[2]

INAF - Osservatorio Astronomico di Torino, Strada Osservatorio 20, 10025 Pino Torinese (TO), Italy

Schelte J. Bus

Institute for astronomy, 640 North A'ohoku Place, Hilo, HI 96720, USA

[1]Partly based on observations obtained at ESO La Silla Observatory, Chile.

[2]Present address: Observatoire de la Côte d'Azur, B.P. 4229, 06304 Nice Cedex 4, France

Submitted to *Icarus*

REVISED II: 8. Dec. 2006

No. of manuscript pages: 38

No. of figures: 5

No. of tables: 5

Running head: **Physical Characterization of NEA 1998 WT_{24}**

Editorial correspondence to:

Alan W. Harris

DLR Institute of Planetary Research

Rutherfordstrasse 2

12489 Berlin

Germany

Tel: +49 30 67055 324

Fax: +49 30 67055 340

E-mail: alan.harris@dlr.de

Abstract

The potentially-hazardous asteroid (33342) 1998 WT_{24} approached the Earth within 0.0125 AU on 2001 Dec. 16 and was the target of a number of optical, infrared, and radar observing campaigns. Interest in 1998 WT_{24} stems from its having an orbit with an unusually low perihelion distance, which causes it to cross the orbits of the Earth, Venus, and Mercury, and its possibly being a member of the E spectral class, which is rare amongst near-Earth asteroids (NEAs). We present the results of extensive thermal-infrared observations of 1998 WT_{24} obtained in December 2001 with the 3-m NASA Infrared Telescope Facility (IRTF) on Mauna Kea, Hawaii and the ESO 3.6-m telescope in Chile. A number of thermal models have been applied to the data, including thermophysical models that give best-fit values of 0.35 ± 0.04 km for the effective diameter, 0.56 ± 0.2 for the geometric albedo, p_v, and 100 – 300 J m^{-2} $s^{-0.5}$ K^{-1} for the thermal inertia. Our values for the diameter and albedo are consistent with results derived from radar and polarimetric observations. The albedo is one of the highest values obtained for any asteroid and, since no other taxonomic type is associated with albedos above 0.5, supports the suggested rare E-type classification for 1998 WT_{24}. The thermal inertia is an order of magnitude higher than values derived for large main-belt asteroids but consistent with the relatively high values found for other near-Earth asteroids. A crude pole solution inferred from a combination of our observations and published radar results is $\beta = -52^{\circ}$, $\lambda = 355^{\circ}$ (J2000), but we caution that this is uncertain by several tens of degrees.

Keywords: Asteroids, Infrared Observations, Photometry, Spectrophotometry

1. Introduction

In recent years near-Earth asteroids (NEAs) have become targets both for Earth-based astronomical observation campaigns and in situ investigations via space missions. The recent missions NEAR-Shoemaker to (433) Eros and Hayabusa to (25143) Itokawa have provided a wealth of fascinating information on two very different NEAs. The results of studies to date have demonstrated that the NEA population has extremely diverse physical characteristics. In particular, NEAs appear to vary widely in terms of shape, mineralogy, albedo, regolith, and other surface properties.

Interest in NEAs arises not only from the potential impact hazard they present to Earth but also from their relation to main-belt asteroids. Most NEAs are thought to be fragments from collisions in the main asteroid belt and are at the large end of a size continuum of material delivered into near-Earth space, which includes meteoroids and interplanetary dust. NEAs are vehicles by means of which material can be transported from the main belt to the inner Solar System and, together with comets, are thought to have played a major role in the development of the surfaces of the inner planets, including the delivery of materials to the Earth that may have contributed to the development of life.

A combination of dynamical processes, including the Yarkovsky effect (see Bottke et al., 2002, and references therein) and mean-motion resonances, enables collisional fragments from different regions of the main belt to reach the inner Solar System. The diversity of the NEA population therefore largely reflects the diversity of the main-belt population. However, NEAs display a particularly broad range of albedo (published values range from 0.02 to 0.6, e.g. see Delbó et al., 2003), which may be due to there being a significant number of dormant or extinct cometary nuclei with very low geometric albedos (p_v = 0.02 – 0.05) amongst the NEAs (e.g.

Binzel et al., 2004), and the possibility that NEAs that are fragments from collisions in the main belt are younger and have generally fresher, less space-weathered (and therefore brighter) surfaces than observable main-belt asteroids (space weathering appears to lead to a darkening of, in particular, olivine-rich surfaces – see Clark et al., 2002, and references therein). However, the taxonomic class associated with the highest albedos is the E class, members of which have albedos typically in the range $p_v = 0.3 – 0.6$. Examples of main-belt E-types are 44 Nysa (IRAS $p_v = 0.55$, Tedesco et al., 2002b), 64 Angelina ($p_v = 0.40$, Tedesco et al., 2002a) and 214 Aschera (IRAS $p_v = 0.52$, Tedesco et al., 2002b); the NEA 3103 Eger has E-type spectral properties (Clark et al., 2004, Gaffey et al., 1992), and on the basis of their thermal-infrared determinations of size and albedo Delbó et al. (2003) suggest E-type classifications for the NEAs 4660 Nereus ($p_v = 0.55$) and 5751 Zao ($p_v = 0.36$). Furthermore, NEA (10302) 1989 ML, previously classed as an X type, has E-type spectral properties and an E-type albedo of $p_v = 0.4$ (Mueller et al., 2006b).

(33342) 1998 WT_{24} was discovered on 1998 Nov. 25 by the LINEAR (Stokes et al., 2000) search program. Observations of physical characteristics published to date suggest that 1998 WT_{24} is a rare E-type Aten NEA with a high polarimetric albedo of around 0.4 (Lazzarin et al., 2004; Kiselev et al., 2002). Krugly et al. (2002) report a rather short rotation period of 3.697 h and a lightcurve amplitude measured at solar phase angles between 50˚ and 60˚ of 0.26 mag. The absolute magnitude at maximum brightness derived by Kiselev et al. (2002) is 18.69 ± 0.08 mag, or 18.39 ± 0.08 mag if a brightness opposition effect is assumed similar to that observed for the E-type asteroids (44) Nysa and (64) Angelina. Given the reported 0.53 mag lightcurve amplitude at the time of the Kiselev et al. photometric observations (2001 Dec. 2 – 9), the Kiselev at al. result of $H_{max} = 18.39 \pm 0.08$ mag is compatible with H (lightcurve mean) = 18.54 ± 0.1 mag derived independently by Delbó (2004) using the method of Bowell et al. (1989) on observations made at ESO on 2001 Dec. 2 and 4, taking G = 0.4. Taking H = 18.5 ±

0.3, the diameter of (33342) 1998 WT_{24} inferred from an albedo of $p_v = 0.4$ is D = 0.42 ± 0.06 km. It should be noted, however, that the derivation of albedos from polarimetric observations is based on a method that depends on empirically derived relations between the polarization parameters and the solar phase angle and albedo and that different calibrations of this method have been published, most recently by Cellino et al. (1999). Kiselev et al. (2002) used the relations of Lupishko and Mohamed (1996). If we take the Kiselev et al. value of $h_v = 0.039$ % deg^{-1} for the slope of the linear part of the polarization-phase curve and apply the appropriate relation of Cellino et al. (1999), we find a higher albedo of $p_v = 0.62$. Assuming H = 18.5 ± 0.3, the implied diameter is reduced to D = 0.34 ± 0.05 km.

Goldstone radar images of 1998 WT_{24} made available on the web by S. Ostro and colleagues (http://neo.jpl.nasa.gov/images/1998wt24.html) suggest a slightly elongated body with a possible concavity. However, no formal report of the Goldstone observations is available at the time of writing. Zaitsev et al. (2002) made radar observations of 1998 WT_{24} on 2001 Dec. 16 and 17 and derived lower limits for the *maximum* pole-on breadth of the asteroid of D_{max} = 0.42 and 0.40 km, respectively, from observations of the Doppler-broadened echo bandwidth, B, on the two dates. B is proportional to D_{max} x sin φ, where φ is the angle between the spin vector and the radar line of sight. Since the pole orientation of 1998 WT_{24} is unknown, only a lower limit for the maximum pole-on dimension can be determined from the radar data.

Further information on the diameter and albedo of 1998 WT_{24} can be obtained from thermal-infrared observations and the application of suitable thermal models. Furthermore, thermal-infrared observations can provide insight into the near-surface thermal inertia and regolith structure, information relevant to modeling the Yarkovsky effect and impact-hazard mitigation techniques. Delbó et al. (2003) used the 10-m Keck-1 telescope for a study of the thermal emission from NEAs. They derived diameters and albedos for 20 NEAs in the size range 0.1 –

10 km and found evidence that most of the observed objects have a significant insulating regolith, rather than a high-thermal-inertia surface characteristic of bare rock. Harris et al. (2005) derived the size, albedo, and thermal inertia of the NEA (1580) Betulia from 7 – 21 μm observations with the NASA Infrared Telescope Facility (IRTF). In the case of Betulia the thermal inertia was found to be intermediate between that of main belt asteroids (5 – 25 J m^{-2} $s^{-0.5}$ K^{-1}, e.g. Müller and Lagerros, 1998) and bare rock (~ 2500 J m^{-2} $s^{-0.5}$ K^{-1}, Jakosky, 1986), i.e. consistent with the findings of Delbó et al. (2003).

We observed (33342) 1998 WT_{24} with the ESO 3.6-m telescope and the IRTF in December 2001. Thermal-infrared flux measurements were obtained at wavelengths in the range 7 – 21 μm. The objective of these measurements was to observe 1998 WT_{24} over the very wide range of solar phase angle ($\alpha = 10^{\circ} - 90^{\circ}$) available for this asteroid during its close approach in December 2001. Observations over this period could provide a valuable database for testing thermal models and enabling the surface thermal inertia of a very small asteroid to be determined. However, the first two out of a total of five observing sessions at the IRTF were lost due to bad weather, consequently no observations at $|\alpha| < 60^{\circ}$ could be made. The remaining three IRTF nights were partially compromised by poor weather and instrument problems but the availability of independent data sets from four nights in total with a broad range of observing geometries (see Table 1) has nevertheless enabled substantial, self-consistent results to be derived. We have fitted the resulting flux data with a number of different thermal models, including a thermophysical model, to obtain the size, albedo and magnitude of the thermal inertia. Furthermore, our results combined with published observations constrain the asteroid's spin axis orientation.

2. Observations and data reduction

Observations were performed on 2001 December 4 at the ESO 3.6 m telescope with the Thermal-Infrared Multimode Instrument (TIMMI 2, Reimann et al., 2000) in imaging mode, and on 2001 December 18, 19 and 21 with the IRTF and JPL's 128 x 128 pixel, 7 - 25 μm infrared astronomical camera, MIRLIN. For details of MIRLIN see Ressler et al. (1994) and http://cougar.jpl.nasa.gov/mirlin.html. The ESO measurements were made in filters centered at 8.73, 10.38, and 11.66 μm with bandwidths of around 10%. The IRTF measurements were made in filters centered at 7.91, 10.27, and 11.7 μm with bandwidths of around 10% and at 17.93 and 20.81 μm with bandwidths of 2.5% and 7.8%, respectively. At each observing site the telescope was tracked at the rates predicted from the ephemerides of the target and the usual chop-nod procedure was used. In each case calibration stars were chosen to be close on the sky to the target asteroid. Standard synthetic aperture procedures were used for the derivation of raw signal counts from the camera images. Absolutely calibrated fluxes for the target asteroids were obtained by multiplying the integrated in-band absolute fluxes of the calibration stars by the ratios of the target/calibration star raw counts in each filter. Absolutely calibrated infrared spectra for the calibration stars β And, α Tau (Dec. 18, 19, 21) and HD 81420 (Dec. 4) were taken from the database of Cohen et al. (1999). Color corrections for the different flux distributions of the calibration stars and asteroids in the narrow filter pass bands were found to be no more than a few percent and were not applied.

Table 1 lists the observing geometry. The resulting fluxes are listed in Table 2. The quoted uncertainties in the flux measurements refer to the formal statistical uncertainties in the synthetic aperture procedure only. The quality of the data is variable due to fluctuating atmospheric and instrumental circumstances. In particular, the Dec. 18 observations were affected by partially non-photometric conditions and problems with the filter wheel. The

scatter of multiple measurements made in the same filter (e.g. see Fig. 1) reveals the presence of non-statistical variability in the data, which is probably due mainly to rotation of the asteroid and variable atmospheric conditions. However, our model fitting routines effectively take account of the scatter in multiple measurements, in addition to the statistical uncertainties, and weight the data accordingly, which mitigates against serious errors due to non-statistical variability.

3. Thermal-model fitting

3.1. Simple models

The high solar phase angles of the observations imply that simple models, such as the standard thermal model (STM, see Lebofsky et al. 1986, and references therein), are likely to give erroneous results. The STM is the basic and most widely used asteroid thermal model; it is based on spherical geometry and was designed for use with main-belt asteroids at solar phase angles $\alpha \leq 30^{\circ}$. The STM may be an appropriate model if the asteroid is rotating slowly and has a low thermal inertia (or its rotation axis points to the Sun) so that each surface element can be considered to be in instantaneous thermal equilibrium with insolation. In the case of 1998 WT_{24} the relatively short rotation period of 3.697 h (e.g. Krugly et al., 2002), and the high values of thermal inertia (relative to those of main-belt asteroids) found recently for NEAs (e.g. see Harris et al., 2005), together with the high phase angles at which the observations were made, indicate that the STM is not an appropriate thermal model.

A corresponding simple model for the extreme case of high thermal inertia and/or fast rotation is the so-called fast rotating or isothermal latitude model (Veeder et al., 1989; Lebofsky and

Spencer, 1989), hereafter FRM, in which the surface temperature distribution is a function of latitude only. An asteroid with a surface of bare rock would be expected to have a high thermal inertia. For objects with significant thermal inertia the FRM can give a useful indication of diameter, especially at high phase angles (see Harris, 2006). The FRM assumes the Sun is in the equatorial plane; if the sub-Earth latitude is also zero, as is normally assumed in the FRM, no phase-angle correction is required.

The near-Earth asteroid thermal model, NEATM (Harris, 1998), can provide useful estimates of diameter and albedo when parameters are intermediate to those for which the STM and FRM are applicable. The STM and the NEATM both incorporate a so-called "beaming parameter", η, which was originally introduced to allow the model temperature distribution to be modified from that of a smooth, zero-thermal-inertia sphere to take account of the observed enhancement of thermal emission at small solar phase angles due to surface roughness. In the STM η has the fixed value of 0.756, whereas in the NEATM η is treated as a modeling parameter that allows a first-order correction for effects such as beaming, thermal inertia and rotation that influence the surface temperature distribution presented to the observer. Changing η causes the effective color temperature, or flux distribution, of the model thermal continuum to change. In the case of the NEATM the value of η giving the best fit to the measured continuum flux distribution is found via an iterative procedure. Unlike the STM and FRM, the NEATM requires measurements of the thermal flux at more than one wavelength because the NEATM treats η as an additional variable (in the cases of the STM and the FRM the only free parameters are diameter and geometric albedo, therefore one measurement in the thermal infrared and one in the visible suffice for a solution).

The value of η resulting from application of the NEATM can be considered a measure of the extent to which the surface temperature distribution departs from that of a perfect STM-type

asteroid (i.e. smooth, with zero thermal inertia), for which $\eta = 1$. At small phase angles $\eta > 1$ indicates significant thermal inertia, whereas $\eta < 1$ indicates significant beaming due to surface roughness. At large phase angles, however, thermal inertia and roughness can both lead to increased η, and detailed thermophysical modeling is required to unravel their contributions.

The NEATM takes account of the phase angle by numerically integrating the observable thermal emission from the spherical surface that is illuminated by the Sun, assuming that surface emits with a Lambertian angular distribution. Since the NEATM and the STM assume that no emission originates on the night side of the object, these models would be expected to lead to overestimation of diameters and underestimation of albedos at very high solar phase angles for objects with high thermal inertia. In such cases the FRM may be the more appropriate model to use.

For more detailed discussions of the NEATM and other thermal models outlined here see Harris (1998), Delbó and Harris (2002), Harris and Lagerros (2002), Delbó et al. (2003), and Harris (2006), and references therein. Delbó and Harris (2002) give the mathematical expressions for calculating the wavelength-dependent observable thermal-infrared fluxes for all three models.

3.2. Thermophysical models

We find it instructive to apply various types of thermal model to thermal-infrared asteroid data to probe the relative accuracies of the different modeling approaches, especially when estimates of size and albedo are available from other techniques such as radar and optical polarimetry. Thermophysical models include phenomena such as thermal inertia, surface roughness (the "beaming effect"), and rotational state explicitly as model parameters and are

potentially more accurate than the simple models described above. However, the extra complexity of thermophysical models is rarely warranted unless a realistic shape model of the object is available. Unfortunately, this is not currently the case for 1998 WT_{24}. Information from radar observations and optical lightcurve observations is available, however, from which some inferences about shape can be made.

Given the variable data quality in the case of 1998 WT_{24}, and the large increases in phase angle between successive observing runs, we decided to take a cautious approach initially and analyze the data on a night-to-night basis to check the data set for consistency and to monitor the performance of the thermophysical approach. For a first thermophysical analysis we adopted a smooth sphere as a shape model (for convenience we refer to this model as the "smooth-sphere" thermophysical model). In the case of 1998 WT_{24}, as with most asteroids, we have no knowledge of detailed topographical structure, which could influence shadowing patterns and the temperature distribution on the surface, and which would be more significant at high phase angles, such as those at which our IRTF observations were made. The standard idealistic treatment of roughness as a uniform distribution of hemispherical craters may be appropriate for large main-belt asteroids, but in the case of very small asteroids its validity is questionable, particularly at high phase angles. In any case, Lagerros (1997) found that the effects of shape tend to dominate those of surface roughness in thermophysical models. In the absence of a more appropriate alternative approach, we chose to ignore surface roughness in the first stage of our thermophysical analysis.

In the second stage of the analysis we explored the effect on the results of a distribution of hemispherical craters by application of our independently developed general thermophysical model, which has been used in earlier studies (e.g. Harris, et al., 2005). The smooth-sphere thermophysical model and the more detailed general thermophysical model both include a

treatment of thermal inertia: the temperature of each surface element is determined by numerically solving the one-dimensional heat diffusion equation. In the more detailed model, which is based on the work of Lagerros (1996, 1998), the surface temperature distribution is further modified by a distribution of hemispherical craters over the surface, with shadowing and multiple reflections of incident solar and thermally emitted radiation inside craters taken account of. The total observable thermal emission is calculated by summing the contributions from each surface element visible to the observer. Model parameters are adjusted until good agreement is obtained with the observational data, thereby constraining the physical properties of the asteroid.

4. Results

4.1. Rotational variability

Due to rotation the observed reflected and emitted radiation from an asteroid vary with time. It is important to take account of the rotational variability in observational data when applying thermal models. When simple models based on spherical geometry are used, optical lightcurves are often used as the basis for correcting thermal-infrared data, a practice that can introduce errors if the optical and thermal-infrared lightcurves are out of phase or differ in structure. Differences in the lightcurves of reflected and emitted radiation can arise from the effects of shape, surface structure and thermal inertia. A further effect, which is important in our study, is the change in the nature of the lightcurve with increasing solar phase angle. Krugly et al. (2002) observed a modest lightcurve amplitude of 0.26 mag at solar phase angle $\alpha = 50^{\circ} - 60^{\circ}$, while Kiselev et al. (2002) observed a lightcurve amplitude of 0.53 mag at $\alpha = 83^{\circ}$. To our knowledge no studies of the phase-dependence of thermal-infrared lightcurves have

been carried out. In the case of (1580) Betulia the optical and thermal-infrared lightcurves at α = 53˚ appear to be quite similar, especially in terms of amplitude (Harris et al., 2005), but comparisons at very high phase angles are lacking. In the case of our IRTF observations of 1998 WT_{24} the solar phase angle was very high and changed significantly from night to night. Rotational variability of the flux values can alter the relative measurements obtained at different wavelengths and therefore influence the results from the model fitting, e.g. lead to erroneous values of η in the case of the NEATM. We note that in the case of the IRTF observations on 2001 Dec. 18, 19, 21 the duration of the observing period on each night was comparable to the time difference between maxima and minima in the lightcurve (see Table 2; a quarter of the period ≈ 55 min), therefore observations probably spanned a large part of the lightcurve amplitude. However, the fact that in general observations in each filter were repeated on each night tends to reduce the chance of non-statistical variability between measurements in different filters causing serious errors in color temperature. The approach we have taken is to apply the various thermal models to the independent uncorrected data sets obtained on each of the four nights and review the consistency of the results.

4.2. Spin vector

An important input parameter for thermophysical modeling of asteroids is the orientation of the rotation axis. In the case of 1998 WT_{24} the rotation rate is well established but no pole solution has been published to date. However, some clues concerning the pole direction can be derived from our data and the published results of other observers. For instance, the value given by Zaitsev et al. (2002) for the *lower bound* on the maximum pole-on breadth of the asteroid from observations of the Doppler-broadened radar echo bandwidth (0.41 km) is very similar to the effective diameter of the asteroid (0.40 km) derived from the polarimetric data of Kiselev et al. (2002) using the Lupishko and Mohamed (1996) calibration, which gives the larger size (see

Section 1). The result of Zaitsev et al. is a lower bound because the actual value of the maximum pole-on breadth is given by 0.41/sin φ km, where φ is the angle between the spin vector and the radar line of sight. Given the similarity between the radar lower bound and the maximum size determined via polarimetry, and the fact that the radar data seem to indicate a near spherical shape, we can infer that the spin vector was not far from being perpendicular to the radar line of sight (or, equivalently, the sub-radar latitude was small). Furthermore, the results of our analyses of the thermal-infrared data obtained over a broad phase-angle range indicate (see Section 4.3) that the rotation axis was oriented nearly perpendicular to the solar direction, that is the sub-solar latitude was small. To simultaneously satisfy the conditions of small sub-Earth and sub-solar latitudes at the time of the radar observations (2001 Dec. 17.0 UT), the coordinates of the pole solution of 1998 WT_{24} must be around $\beta = 52^{\circ}$, $\lambda = 175^{\circ}$ or $\beta = -52^{\circ}$, $\lambda = 355^{\circ}$ (J2000), depending on whether the rotation is prograde or retrograde, respectively. Note, however, that the above reasoning allows only very crude indications of the pole orientation to be inferred; the quoted solutions may be in error by several tens of degrees.

4.3. Simple models

The results of fitting the NEATM and FRM to the four 2001 December data sets are presented in Table 3. The FRM best-fit diameter is reasonably consistent in all cases, while the NEATM best-fit diameter varies between 0.31 km and 0.62 km. The FRM assumes that the rotation axis is perpendicular to the plane containing the Sun, asteroid and observer, so consistency of the FRM results leads us to infer that the sub-solar latitude was small throughout the period of the infrared observations. If this were not the case, we would expect the FRM to give erroneously large diameters at lower phase angles due to the increased visibility from the Earth of warm surface areas at high asteroidal latitudes (see Harris, 2006). For an FRM-type asteroid, i.e. fast

rotating with low sub-solar and sub-Earth latitudes, the thermal emission observed is independent of solar phase angle.

As discussed in Section 3.1, for objects with significant thermal inertia the NEATM would be expected to overestimate diameters at large phase angles due to emission arising from the night side of the object (the NEATM assumes *observed* thermal emission is from the day side only, which is approximately true if the object is observed at a moderate phase angle, or has low thermal inertia/is a slow rotator, or the sub-solar latitude is near 90˚).

The above considerations allow constraints to be applied to the size of 1998 WT_{24} from the NEATM and FRM results. In the case of NEATM the lower phase angle (60˚, 79˚) results of Dec. 4 and Dec. 19 can be taken as an upper limit, i.e. $D_{NEATM} < 0.41$ km (note that the results of Dec. 18 may have been compromised by poor quality data due to weather and instrument problems – see Section 2). In the case of the FRM the highest phase angle (93˚) results, which should be the most reliable, give $D_{FRM} = 0.36$ km.

4.4. Thermophysical models

We initially applied the smooth-sphere thermophysical model described in Section 3.2. An example of the scatter of the flux values and the difficulty in determining best-fit parameters for a single data set is shown in Fig. 1. We assumed the pole direction discussed in Section 4.2 and tried both prograde and retrograde rotation states, in each case calculating best fit diameters for 7 different values of thermal inertia in the range 10 – 1000 J m^{-2} $s^{-0.5}$ K^{-1}. For comparison, values of thermal inertia measured to date for large main-belt asteroids are around 5 – 25 J m^{-2} $s^{-0.5}$ K^{-1} (Müller and Lagerros, 1998), while the highest value published to date is 750 J m^{-2} $s^{-0.5}$ K^{-1} for the NEA (25143) Itokawa (Müller et al., 2005). Note that the sense of the

solar phase angle changed on Dec. 15. For example, if rotation is retrograde the cooler morning side of the asteroid was observed prior to Dec. 15 and the warmer afternoon side after Dec. 15. The converse applies in the prograde case.

For each value of thermal inertia and each of the four nights of observations the value of diameter minimizing reduced χ^2 was calculated (see Table 4), where

$$\text{reduced } \chi^2 = \sum [(F_n(\text{obs}) - F_n(\text{model}))/\sigma_n]^2 / (n-2) \quad (1)$$

and n is the number of flux measurements, 2 is the number of free parameters in the fit (diameter and thermal inertia), and σ_n are the statistical uncertainties in the photometry, F_n(obs). In the following χ^2 refers to reduced χ^2. Note that the scatter of the flux values about the best-fit model thermal continua (see Fig. 1) reflects atmospheric variability and lightcurve effects, in addition to the statistical errors given in Table 2, so the values of χ^2_{min} in Table 4 are generally well above unity. The mean diameters and corresponding standard deviations for each value of thermal inertia are listed in the respective columns of Table 4. In addition, we list the value of $\Sigma\Delta\chi^2$, which is the sum over the four data sets of the differences between χ^2_{min} for each value of thermal inertia and the overall lowest χ^2_{min} for the corresponding date. Taking the results for Dec. 19 (retrograde case) for example, the overall lowest χ^2_{min}, 10.2, is obtained for a thermal inertia value of 50 J m^{-2} s$^{-0.5}$ K^{-1}, so $\Delta\chi^2$ in the case of thermal inertia = 1000 J m^{-2} s$^{-0.5}$ K^{-1} is 16.4 – 10.2 = 6.2, so the relatively poor fit obtained with the high value of thermal inertia incurs a relatively large penalty ($\Delta\chi^2$ = 6.2). In contrast, for Dec. 4 the corresponding value of $\Delta\chi^2$ is only 0.14, because the poorer data set of Dec. 4 does not allow confident discrimination between different values of thermal inertia.

The minimum value of $\Sigma\Delta\chi^2$, i.e. 2.22, corresponds to the overall best-fitting thermal inertia of 100 J m^{-2} $s^{-0.5}$ K^{-1} for the combined data of all four nights (Fig. 2). The corresponding mean diameter is 0.33 km (0.34 km if the poor quality data of Dec. 18 are excluded) and we see that this value also corresponds to the minimum scatter in diameter for the four dates (Fig. 3), i.e. this value of diameter, with a thermal inertia of 100 J m^{-2} $s^{-0.5}$ K^{-1}, and retrograde rotation, appears to give the most consistent fits to the data. Considering the results for prograde rotation in the lower part of Table 4, it is clear that no combination of thermal inertia and diameter gives a comparably convincing overall result.

In summary, the results from the smooth-sphere thermophysical model are: D_{eff} = 0.34 ± 0.02 km, p_v = 0.60 ± 0.2 (assuming H = 18.5 ± 0.3), and thermal inertia ~ 100 J m^{-2} $s^{-0.5}$ K^{-1}, which are consistent with those from the FRM and NEATM. In Fig. 1 best-fit model thermal continua for thermal inertia values of 10, 100, and 1000 J m^{-2} $s^{-0.5}$ K^{-1} are shown superimposed on the flux measurements of 2001 Dec. 19.

Finally we applied the more detailed general thermophysical model, which explicitly takes account of the shape, spin vector and surface roughness, in addition to thermal inertia, as described in Section 3.2. This model, or a similar one, has been applied in the analysis of thermal-infrared data for (25143) Itokawa (Mueller et al., 2006a; Müller et al., 2005) and (1580) Betulia (Harris et al., 2005). Since no shape model has yet been published for 1998 WT_{24}, we first tried modeling the asteroid as a biaxial ellipsoid spinning about one of the two shorter axes. The ellipsoid was modeled as a mesh of 6144 triangular facets. Several types of ellipsoid were tried, all of which were consistent with published optical lightcurves, but the results turned out to be largely independent of the shape of the ellipsoid. In fact, it was found that no ellipsoid fitted the thermal data significantly better than a sphere. Therefore, we pursued our analysis using the general thermophysical model, based on a sphere, to test the

effects of surface roughness and to check the results obtained with the completely independent smooth-sphere thermophysical model described above. Surface roughness is modeled as a uniform distribution of craters (hemispherical sections); the degree of roughness is varied by changing the crater density and the crater opening angle. Shadowing and multiple reflections of incident solar and thermally emitted radiation inside craters are taken into account.

For both possible spin directions (see Section 4.2) surface roughness, thermal inertia, and size were adjusted until the best agreement was obtained with the full set of observational results listed in Table 2, i.e. χ^2 was minimized. It was found that the fit significantly improved when the data from Dec. 18 were excluded, which is consistent with these data being of inferior quality, as discussed above.

As in the case of the smooth-sphere thermophysical model, the retrograde pole solution was found to fit the data significantly better than the prograde solution. For the retrograde pole solution, and different degrees of surface roughness, the best-fit thermal inertia is about 200 J m^{-2} $s^{-0.5}$ K^{-1}, with an uncertainty of some 100 J m^{-2} $s^{-0.5}$ K^{-1} (Fig. 4). Zero roughness and the highest degree of roughness (saturated crater coverage) give slightly worse fits to the data. In the case of zero roughness we note that the more detailed general thermophysical model gives very similar results to those of the independently developed smooth-sphere model. The corresponding best-fit values of diameter and albedo are 0.35 ± 0.02 km and $p_v = 0.56 \pm 0.2$ (assuming H = 18.5 ± 0.3). Figure 5 illustrates the dependence of diameter on roughness and thermal inertia.

5. Uncertainties

The error bars in the plot of Fig. 1 reflect only the statistical uncertainties in the flux derivation from the synthetic aperture procedure. Absolute calibration uncertainties, differences in atmospheric transmission between measurements of the target and calibration star, and lightcurve effects, also contribute to the error budget.

Uncertainties in thermal modeling usually exceed the formal errors resulting from the scatter of the flux measurements. In the case of NEATM, comparison with results from other sources, such as radar, indicate that overall errors are normally less than 15% in diameter and 30% in albedo. In the case of a very irregularly shaped object, or one with complex large-scale surface topography, errors may be larger; at large phase angles an additional error arises due to radiation emitted on the night side, as discussed in Section 3.1. The uncertainty in the adopted H-value increases the uncertainty in derived values of albedo but has relatively little effect on the uncertainty in the diameter.

Comparison with independent results for D_{eff} in the cases of (433) Eros and (25143) Itokawa suggests the uncertainty in diameter determinations with the more detailed general thermophysical model is around 10%. Further testing of the model is required to refine the uncertainty estimates.

6. Discussion

The results of the more detailed general thermophysical model should be the most robust, although the accuracy of thermophysical modeling depends crucially on the accuracy and

resolution of the shape model used. Unresolved topographic structure, such as large concavities or boulders, could influence the temperature distribution on the surface, and would be more significant at the high phase angles of our observations. So we caution that the modeling uncertainties in our results are considerable. Nevertheless, despite the fact that all the thermal models used have their shortcomings and have not been thoroughly tested at the high phase angles of our 1998 WT_{24} observations, the overall agreement of the results from the various models is good.

Zaitsev et al. (2002) derived lower limits for the maximum pole-on breadth of 0.42 and 0.40 km, respectively, from observations of the Doppler-broadened radar echo bandwidth on two consecutive dates. Zaitsev et al. interpret the constancy of their radar echo bandwidths as indicating a roughly spherical shape. The lightcurve amplitude of 0.26 mag peak to peak reported by Krugly et al. (2002) at phase angles between 50˚ and 60˚, suggests an axial ratio of roughly a/b = 1.15, after reducing the lightcurve amplitude by a factor of 1.7 to crudely correct for the phase-angle dependence (Zappala et al., 1990). Given the effective diameter of 0.35 km derived in this work, the corresponding dimensions of a biaxial ellipsoid would be a = 0.38 km and b = 0.33 km. The larger dimension is consistent with the results of Zaitsev et al. (2002), given the uncertainties. We conclude that our results are consistent with published values for the diameter and albedo derived using independent techniques (Table 5), which increases our confidence in the thermal inertia and approximate pole solution derived in this work.

An interesting result from this work is that neglecting surface roughness in the thermal modeling does not alter the results substantially (cf. the entries in Table 5 for the two thermophysical models used). In this respect the thought-provoking images of (25143) Itokawa from the Hayabusa mission (e.g. Saito et al., 2006), which reveal a boulder-strewn surface virtually devoid of craters, leads one to question the validity of the idealistic treatment of

roughness as a uniform distribution of hemispherical craters in the case of very small asteroids. However, in the absence of high-resolution shape models there is currently no alternative. An important area for future work is to study how the accuracy of thermophysical models might be influenced by the presence of intermediate-scale topographic structure, e.g. large concavities and other features intermediate in scale between craters and the whole body that are not normally included in shape models.

Our albedo for 1998 WT_{24} of $p_v = 0.56 \pm 0.2$ is at the high end of the range associated with E types in general and means that this object has one of the highest albedos measured for any asteroid. The uncertainty in our derived albedo is, however, relatively large, due to modeling uncertainties and the uncertainty in the H value. A fainter H value would lead to a lower albedo but would have little influence on the derived diameter. E-type spectra are flat and largely featureless and are thought to be indicative of the spectrally neutral mineral enstatite or other iron-poor silicates. E-type asteroids may have an origin in the crust or exposed mantle of a differentiated parent body (Gaffey et al., 1989) and are relatively rare; only a handful of NEAs have characteristics suggestive of E-class membership, including 3103 Eger, 4660 Nereus, 5751 Zao, and (10302) 1989 ML. E-type asteroids may be sources of the aubrite meteorites, which have similar spectral characteristics (e.g. Lazzarin et al., 2004), although Clark et al. (2004) argue on the basis of spectroscopic observations and compositional modeling that 3103 Eger is unlikely to be a source of the aubrites. 4660 Nereus and 1998 WT_{24} are potentially hazardous objects with inclinations of 1.4° and 7.3°, respectively, that have made close approaches to the Earth in the past. These two NEAs have physical and dynamical characteristics that make them prime candidate sources of the aubrite meteorites.

7. Conclusions

Various models applied to thermal-infrared flux measurements of the near-Earth asteroid 1998 WT_{24} obtained at ESO and the NASA IRTF result in an effective diameter of 0.35 ± 0.04 km and an albedo of $p_v = 0.56 \pm 0.2$ (the conservative uncertainties allow for modeling errors and, in the case of p_v, the uncertainty in H) and indicate that the surface thermal inertia is around 100 – 300 J m^{-2} $s^{-0.5}$ K^{-1}, or a few times the lunar value. The high albedo is consistent with the suggestion that 1998 WT_{24} is a member of the E spectral class; so this NEA, which is a potentially hazardous object with a minimum orbit intersection distance (MOID) of only 0.0097 AU and a modest orbital inclination of 7.3°, should be considered, together with 4660 Nereus, a prime candidate source of the aubrite meteorites. The thermal inertia is much lower than that expected for a bare-rock surface and implies that 1998 WT_{24} has significant areas of thermally insulating regolith. Our results suggest that 1998 WT_{24} is a retrograde rotator. A crude pole solution inferred from a combination of our results and the radar observations of Zaitsev et al. (2002) is $\beta = -52^{\circ}$, $\lambda = 355^{\circ}$ (J2000), but we caution that this is uncertain by several tens of degrees.

Our results are consistent with those of Delbó et al. (2003), Mueller et al. (2006a), and Harris et al. (2005), which indicate that near-Earth asteroids generally have moderate thermal inertias, indicative of surfaces with some exposed rock but largely covered in thermally insulating regolith or dust.

Acknowledgments

The comments and suggestions of the reviewers, anonymous and Stephan Price, are gratefully acknowledged. Most of the data presented herein were obtained with the Infrared Telescope Facility, which is operated by the University of Hawaii under Cooperative Agreement no. NCC 5-538 with the National Aeronautics and Space Administration, Office of Space Science, Planetary Astronomy Program. The work of M. Delbó and M. Mueller was partly supported by the Deutsche Forschungsgemeinschaft (DFG). Liberal use was made of the excellent JPL Horizons System for generating ephemerides.

References

Binzel, R. P., Rivkin, A. S., Stuart, J. S., Harris, A. W., Bus, S. J., Burbine, T. H., 2004. Observed spectral properties of near-Earth objects: results for population distribution, source regions, and space weathering processes. Icarus 170, 259 – 294.

Bottke, W. F., Vokrouhlicky, D., Rubincam, D. P., Broz, M., 2002. The effect of Yarkovsky thermal forces on the dynamical evolution of asteroids and meteoroids. In: Bottke, W.F., Cellino, A., Paolicchi, P., and Binzel, R.P. (Eds.), Asteroids III. Univ. of Arizona Press, Tucson, pp. 395–408.

Bowell, E., Hapke B., Domingue D., Lumme K., Peltoniemi J., Harris A. W., 1989. Application of photometric models to asteroids. In: Binzel, R.P., Gehrels, T., Matthews, M. S., (Eds.), Asteroids II. Univ. of Arizona Press, Tucson, pp. 524 - 556.

Cellino, A., Gil Hutton, R., Tedesco, E. F., Di Martino, M., Brunini, A., 1999. Polarimetric observations of small asteroids: preliminary results. Icarus 138, 129 – 140.

Clark, B. E., Hapke, B., Pieters, C., Britt, D., 2002. Asteroid space weathering and regolith evolution. In: Bottke, W.F., Cellino, A., Paolicchi, P., and Binzel, R.P. (Eds.), Asteroids III. Univ. of Arizona Press, Tucson, pp. 585 –599.

Clark, B. E., Bus, S. J., Rivkin, A. S., McConnochie, T., Sanders, J., Shah, S., Hiroi, T., Shepard, M., 2004. E-type asteroid spectroscopy and compositional modeling. J. Geophys. Res. 109, E02001.

Cohen, M., Walker, R.G., Carter, B., Hammersley, P., Kidger, M., Noguchi, K., 1999. Spectral irradiance calibration in the infrared. X. A self-consistent radiometric all-sky network of absolutely calibrated stellar spectra. Astron. J. 117, 1864 – 1889.

Delbó, M., 2004. Ph.D. dissertation, Free University of Berlin.

Delbó, M., Harris, A. W., 2002. Physical properties of near-Earth asteroids from thermal infrared observations and thermal modeling. Meteoritics and Plan. Sci. 37, 1929–1936.

Delbó, M., Harris, A. W., Binzel, R. P, Pravec, P., Davies, J. K., 2003. Keck observations of near-Earth asteroids in the thermal infrared. Icarus 166, 116 – 130.

Gaffey, M. J., Bell, J. F., Cruikshank, D. P., 1989. Reflectance spectroscopy and asteroid surface mineralogy. In Asteroids II (R. P. Binzel, T. Gehrels, M. S. Matthews, Eds.), pp. 98 - 127. Univ. of Arizona Press, Tucson.

Gaffey, M. J., Reed, K. L., Kelley, M. S., 1992. Relationship of E-type Apollo asteroid 3103 (1982 BB) to the enstatite achondrite meteorites and the Hungaria asteroids. Icarus 100, 95 – 109.

Harris, A. W., 1998. A thermal model for near-Earth asteroids. Icarus 131, 291–301.

Harris, A. W., 2006. The surface properties of small asteroids from thermal-infrared observations. In: Lazzaro, D., Ferraz-Mello, S., Fernández, J. A. (Eds.), Proc. of IAU Symposium 229. Cambridge University Press, Cambridge, pp. 449 – 463.

Harris, A. W., Lagerros, J. S. V., 2002. Asteroids in the thermal infrared. In: Bottke, W.F., Cellino, A., Paolicchi, P., Binzel, R.P. (Eds.), Asteroids III. Univ. of Arizona Press, Tucson, pp. 205 – 218.

Harris, A. W., Mueller, M., Delbó, M., Bus, S. J. 2005. The surface properties of small asteroids: peculiar Betulia – a case study. Icarus 179, 95 – 108.

Jakosky, B.M.,1986. On the thermal properties of Martian fines. Icarus, 66, 117–124.

Kiselev, N. N., Rosenbush, V. K., Jockers, K., Velichko, F. P., Shakhovskoj, N. M., Efimov, Y. S., Lupishko, D. F., Rumyantsev, V. V., 2002. Polarimetry of near-Earth asteroid 33342 (1998 WT24). Synthetic phase angle dependence of polarization for the E-type asteroids. In: Warmbein, B. (Ed.), Proc. of the Conference Asteroids, Comets, Meteors ACM 2002, ESA SP-500, ESA, Noordwijk, The Netherlands, pp. 887 – 890.

Krugly, Y. N., Belskaya, I. N., Chiorny, V. G., Shevchenko, V. G., Gaftonyuk, N. M., 2002. CCD photometry of near-Earth asteroids in 2001. In: Warmbein, B. (Ed.), Proc. of the Conference Asteroids, Comets, Meteors ACM 2002, ESA SP-500, ESA, Noordwijk, The Netherlands, pp. 903 – 906.

Lagerros, J. S. V., 1996. Thermal physics of asteroids I. Effects of shape, heat conduction and beaming. Astron. Astrophys. 310, 1011 – 1020.

Lagerros, J. S. V., 1997. Thermal physics of asteroids III. Irregular shapes and albedo variegations. Astron. Astrophys. 325, 1226 – 1236.

Lagerros, J. S. V., 1998. Thermal physics of asteroids IV. Thermal infrared beaming. Astron. Astrophys. 332, 1123 – 1132.

Lazzarin, M., Marchi, S., Barucci, M. A., Di Martino, M., Barbieri, C., 2004. Visible and near-infrared spectroscopic investigation of near-Earth objects at ESO: first results. Icarus 169, 373 – 384.

Lebofsky, L. A., Spencer, J. R., 1989. Radiometry and thermal modeling of asteroids. In: Binzel, R.P., Gehrels, T., Matthews, M. S., (Eds.), Asteroids II. Univ. of Arizona Press, Tucson, pp. 128 – 147.

Lebofsky, L. A., Sykes, M. V., Tedesco, E. F., Veeder, G. J., Matson, D. L., Brown, R. H., Gradie, J. C., Feierberg, M. A., Rudy, R. J., 1986. A refined "standard" thermal model for asteroids based on observations of 1 Ceres and 2 Pallas. Icarus 68, 239 – 251.

Lupishko, D. F., Mohamed, R. A., 1996. A new calibration of the polarimetric albedo scale of asteroids. Icarus 119, 209 – 213.

Mueller, M., Delbó, M., di Martino, M., Harris, A. W., Kaasalainen, M., Bus, S. J., 2006a. Indications for regolith on Itokawa from thermal-infrared observations. ASP Conference Series (in press).

Mueller, M., Harris, A. W., Fitzsimmons, A., 2006b. Size, albedo, and taxonomic type of potential spacecraft target asteroid (10302) 1989 ML. Icarus, submitted.

Müller, T. G., Lagerros, J. S. V., 1998. Asteroids as far-infrared photometric standards for ISOPHOT. Astron. Astrophys. 338, 340 – 352.

Müller, T. G., Lagerros, J. S. V., Burgdorf, M., Lim, T., Morris, P. W., Salama, A., Schulz, B., Vandenbussche, B., 1999. Fundamental thermal emission parameters of main-belt asteroids derived from ISO. In: Cox, P., Kessler, M. F. (Eds.), The Universe as Seen by ISO. ESA SP- 427, ESA, Noordwijk, The Netherlands, pp. 141 – 144.

Müller, T. G., Sekiguchi, T., Kaasalainen, M., Abe, M., Hasegawa, S., 2005. Thermal infrared observations of the Hayabusa spacecraft target asteroid 25143 Itokawa. Astron. Astrophys. 443, 347 – 355.

Reimann, H.-G., Linz, H., Wagner, R., Relke, H., Kaeufl, H. U., Dietzsch, E., Sperl, M., Hron, J., 2000. TIMMI 2: a new multimode mid-infrared instrument for the ESO 3.6 m telescope. Proc. of SPIE 4008, 1132 – 1143.

Ressler, M.E., Werner, M.W., Van Cleve, J., Choa, H. A., 1994. The JPL deep-well mid-infrared array camera. Experimental Astronomy 3, 277 – 280.

Saito, J., and 33 colleagues, 2006. Detailed images of asteroid 25143 Itokawa from Hayabusa. Science 312, 1341 – 1344.

Stokes, G. H., Evans, J. B., Viggh, H. E. M., Shelly, F. C., Pearce, E. C., 2000. Lincoln near-Earth asteroid program (LINEAR). Icarus 148, 21 – 28.

Tedesco, E. F., Egan, M. P., Price, S. D., 2002a. The *Midcourse Space Experiment* Infrared Minor Planet Survey. Astron. J. 124, 583 – 591.

Tedesco, E. F., Noah, P. V., Noah, M., Price, S. D., 2002b. The supplemental *IRAS* minor planet survey. Astron. J. 123, 1056 – 1085.

Veeder, G. J., Hanner, M. S., Matson, D. L., Tedesco, E. F., Lebofsky, L. A., Tokunaga, A. T., 1989. Radiometry of near-Earth asteroids. Astron. J. 97, 1211 – 1219.

Zaitsev, A. L., and 19 colleagues, 2002. Radar detection of NEA 33342 (1998 WT24) with Evpatoria – Medicina System at 6 cm. In: Warmbein, B. (Ed.), Proc. of the Conference Asteroids, Comets, Meteors ACM 2002, ESA SP-500, ESA, Noordwijk, The Netherlands, pp. 883 – 886.

Zappala, V., Cellino, A., Barucci, A. M., Fulchignoni, M., Lupishko, D. F., 1990. An analysis of the amplitude-phase relationship among asteroids. Astron. Astrophys. 231, 548 – 560.

TABLE 1

Observing geometry

33342 1998 WT_{24}	2001 Dec. 04	2001 Dec. 18	2001 Dec. 19	2001 Dec. 21
Telescope	ESO	IRTF	IRTF	IRTF
Heliocentric distance, r (AU)	1.0148	0.9901	0.9874	0.9817
Geocentric distance, Δ (AU)	0.0621	0.0162	0.0198	0.0284
Solar phase angle, α^o	-60.4	67.5	79.3	93.4

Note: The sense of the solar phase angle changed on Dec. 15. For example, if rotation is retrograde (see Section 4), the cooler morning side of the asteroid was observed prior to Dec. 15 and the warmer afternoon side after Dec. 15.

TABLE 2

Measured flux values

Date (UT)	Time (UT)	Julian date (days - 2452240)	Wave-length (μm)	Flux (mJy)	Error (mJy)	Flux (10^{-14} W m^{-2} μm^{-1})	Error (10^{-14} W m^{-2} μm^{-1})
2001-12-04	09:10	7.8819	8.73	144	31	0.545	0.117
	08:53	7.8701	10.38	239	15	0.662	0.042
	08:50	7.8681	11.66	262	37	0.555	0.078
2001-12-18	05:32	21.7306	7.91	2859	246	13.69	1.18
	05:33	21.7312	7.91	3109	265	14.90	1.27
	05:57	21.7479	10.27	5017	189	14.26	0.54
	05:58	21.7486	10.27	4226	161	12.01	0.46
	05:30	21.7292	11.70	4887	83	10.70	0.18
	05:38	21.7347	11.70	4592	121	10.06	0.26
	05:39	21.7354	11.70	5177	92	11.34	0.20
	05:55	21.7465	11.70	4880	91	10.69	0.20
	05:34	21.7319	17.93	5849	1219	5.45	1.14
	05:45	21.7396	17.93	7005	887	6.532	0.827
2001-12-19	05:48	22.7417	7.91	1758	62	8.423	0.297
	06:17	22.7618	7.91	1416	54	6.785	0.259
	06:49	22.7840	7.91	1444	66	6.919	0.316
	05:05	22.7118	11.70	3180	68	6.964	0.149
	05:51	22.7437	11.70	3220	48	7.052	0.105
	06:20	22.7639	11.70	3294	51	7.214	0.112
	06:52	22.7861	11.70	2658	63	5.821	0.138
	05:12	22.7167	17.93	3847	217	3.587	0.202
	05:57	22.7479	17.93	3402	230	3.172	0.214
	06:25	22.7674	17.93	3079	293	2.871	0.273
	06:59	22.7910	17.93	3805	382	3.548	0.356
	05:23	22.7243	20.81	4959	736	3.433	0.510
2001-12-21	04:53	24.7035	7.91	489	50	2.343	0.240
	05:48	24.7417	7.91	546	57	2.616	0.273
	05:01	24.7090	10.27	915	31	2.601	0.088
	05:55	24.7465	10.27	1058	45	3.007	0.128
	05:07	24.7132	11.70	1146	33	2.510	0.072
	06:01	24.7507	11.70	1384	49	3.031	0.107
	05:20	24.7222	17.93	1915	103	1.786	0.096
	06:14	24.7597	17.93	2119	202	1.976	0.188

Note: The database presented here is an updated version of that given by Delbó (2004), who discusses these observations in his dissertation. In an attempt to maximize the accuracy of the data in the present work, we have filtered out cases of bad airmass matching between asteroid observations and those of calibration stars, and observations made at times when cirrus was known to be present.

TABLE 3

Diameter and albedo determinations from the application of the NEATM and the FRM to the data listed in Table 2

Data set	α^o	No. flux points	D_{eff} (km) NEATM	p_v NEATM	η NEATM	Deff (km) FRM	p_v FRM
2001 Dec. 04	-60.4	3	0.40	0.43	1.86	0.38	0.49
2001 Dec. 18	67.5	10	0.31	0.75	0.61	0.39	0.46
2001 Dec. 19	79.3	12	0.41	0.42	1.25	0.38	0.48
2001 Dec. 21	93.4	8	0.62	0.18	2.70	0.355	0.58

Note: The unusually low value of η for Dec. 18 may be indicative of poor quality data or lightcurve effects (see Sections 2 and 4.1). An absolute magnitude of $H = 18.5 \pm 0.3$ mag was adopted (see Section 1). D_{eff} is the diameter of a sphere of equivalent projected area to that of the asteroid at the mean level of the lightcurve. The uncertainties are dominated by modeling uncertainties, especially at the high solar phase angles of our observations, at which NEATM may overestimate the diameter by 10% or more; the error increases with increasing thermal inertia and phase angle (see Harris, 2006). On the other hand, the accuracy of the FRM would be expected to improve with increasing thermal inertia and phase angle.

TABLE 4

Best-fit diameters in km (with corresponding χ^2_{min} in brackets) from the smooth-sphere thermophysical model for various realistic values of thermal inertia (10 - 1000 J m^{-2} s$^{-0.5}$ K^{-1})

	10	50	100	150	200	500	1000
Retrograde							
Dec. 04	0.291 (1.79)	0.318 (1.50)	0.341 (1.26)	0.356 (1.16)	0.365 (1.13)	0.381 (1.23)	0.378 (1.27)
Dec. 18	0.333 (4.46)	0.325 (4.99)	0.321 (5.49)	0.320 (5.87)	0.321 (6.22)	0.335 (7.71)	0.351 (8.98)
Dec. 19	0.362 (11.1)	0.347 (10.2)	0.337 (10.4)	0.332 (10.8)	0.330 (11.2)	0.336 (13.7)	0.347 (16.4)
Dec. 21	0.383 (11.3)	0.356 (7.97)	0.337 (7.35)	0.326 (7.25)	0.320 (7.21)	0.313 (6.89)	0.318 (6.49)
Mean	0.342	0.336	0.334	0.333	0.334	0.341	0.348
S. D.	0.040	0.018	0.009	0.016	0.021	0.029	0.025
$\Sigma\,\Delta\chi^2$	6.37	2.38	2.22	2.80	3.48	7.25	10.86
Prograde							
Dec. 04	0.283 (1.76)	0.281 (1.54)	0.281 (1.39)	0.283 (1.29)	0.286 (1.23)	0.307 (1.07)	0.326 (1.06)
Dec. 18	0.344 (4.43)	0.372 (5.12)	0.394 (6.52)	0.406 (7.97)	0.413 (9.21)	0.416 (12.1)	0.407 (12.4)
Dec. 19	0.377 (11.4)	0.410 (10.5)	0.431 (14.3)	0.438 (19.7)	0.440 (24.2)	0.423 (31.4)	0.404 (29.3)
Dec. 21	0.405 (12.4)	0.442 (6.41)	0.456 (4.46)	0.452 (4.74)	0.445 (5.19)	0.401 (5.50)	0.372 (5.35)
Mean	0.352	0.376	0.391	0.395	0.396	0.387	0.377
S. D.	0.052	0.070	0.077	0.077	0.075	0.054	0.038
$\Sigma\,\Delta\chi^2$	9.54	3.12	6.22	13.25	19.38	29.62	27.66

Notes: $\Sigma\Delta\chi^2$ is the sum over the four data sets of the differences between χ^2_{min} for each value of thermal inertia and the overall lowest χ^2_{min} for the corresponding date. The formal definition of χ^2 is given in Eq. (1).

TABLE 5

Summary of diameter, albedo and thermal inertia determinations for (33342) 1998 WT_{24}.

Source	D_{eff} (km)	p_v	Thermal inertia ($J\ m^{-2}\ s^{-0.5}\ K^{-1}$)	Notes
Kiselev et al. (2002)	0.40 ± 0.13	0.43 ± 0.15	-	p_v from polarimetry (Lupishko and Mohamed, 1996, calibration).
Kiselev et al. (2002)	0.34 ± 0.10	0.62 ± 0.17	-	p_v from polarimetry (Cellino et al., 1999, calibration).
Zaitsev et al. (2002)	(D_{max} > 0.40)	-	-	From radar (lower bound on the maximum pole-on breadth).
Present work	0.35 ± 0.02	0.56 ± 0.2	100 - 300	Using general thermophysical model (see text).
Present work	0.34 ± 0.02	0.60 ± 0.2	~100	Using smooth-sphere thermophysical model (see text).
Present work	~ 0.36	~ 0.54	-	FRM results from data of Dec. 21.
Present work	< 0.41	> 0.42	-	NEATM results from data of Dec. 4, 19.

Note: The value of the absolute magnitude assumed is H = 18.5 ± 0.3. We estimated uncertainties for the polarimetric albedos from the uncertainties in the coefficients of the albedo-polarimetric slope relations (see Cellino et al., 1999). The NEATM would be expected to overestimate diameters at large phase angles due to its assumption that all observed thermal emission is from the day side, therefore an upper limit is quoted here derived from the data taken on Dec. 4 and 19. In contrast to the NEATM, the reliability of the FRM should improve with increasing solar phase angle (see Harris, 2006), thus the entry for the FRM is based on the data from Dec. 21 (α = 93.4˚). The effective diameter, D_{eff}, is the diameter of a sphere of equivalent projected area to that of the asteroid at the mean level of the lightcurve. D_{max} refers to the maximum dimension perpendicular to the rotation axis.

Figure Captions

Figure 1. Weighted best fits of thermal-model continua to the flux data of 2001 December 19. The curves were derived from a spherical thermophysical model, in which retrograde rotation is assumed and surface roughness is ignored, with thermal inertia set at 10 J m^{-2} $s^{-0.5}$ K^{-1} (dotted curve), 100 J m^{-2} $s^{-0.5}$ K^{-1} (dashed curve), and 1000 J m^{-2} $s^{-0.5}$ K^{-1} (continuous curve). The model curves are best fits generated by finding the values of diameter that minimize χ^2. The error bars reflect only the statistical uncertainties in the flux derivation from the synthetic aperture procedure: the scatter of the data points is probably largely due to varying atmospheric transmission and rotational variability (lightcurve effects).

Figure 2. Smooth-sphere thermophysical model: $\Sigma\Delta\chi^2$ versus thermal inertia, where $\Sigma\Delta\chi^2$ is the sum over the four data sets of the differences between χ^2_{min} for each value of thermal inertia and the overall lowest χ^2_{min} for the corresponding date (see text and Table 4). The overall minimum in $\Sigma\Delta\chi^2$ is obtained with a thermal inertia of 100 J m^{-2} $s^{-0.5}$ K^{-1} and retrograde rotation.

Figure 3. Smooth-sphere thermophysical model: Standard deviation of the best-fit diameters for the four observation dates (see Table 4) as a function of thermal inertia. The least dispersion in best-fit diameter over the four dates is obtained with a thermal inertia of 100 J m^{-2} $s^{-0.5}$ K^{-1} and retrograde rotation.

Figure 4. General thermophysical model: Goodness of fit (χ^2) as a function of thermal inertia for retrograde rotation and different degrees of surface roughness (zero, low, default and high roughnesses, where "default" corresponds to roughness parameters determined for large main-belt asteroids – see Müller et al., 1999). The quality of the fit in the cases of zero roughness

and the highest degree of roughness (saturated crater coverage) is slightly worse, otherwise the degree of roughness is not well constrained by the data. The best-fit thermal inertia is 100 – 300 J m^{-2} $s^{-0.5}$ K^{-1}.

Figure 5. General thermophysical model: The dependence of diameter on thermal inertia for different degrees of surface roughness (see caption to Fig. 4).

Figure 1

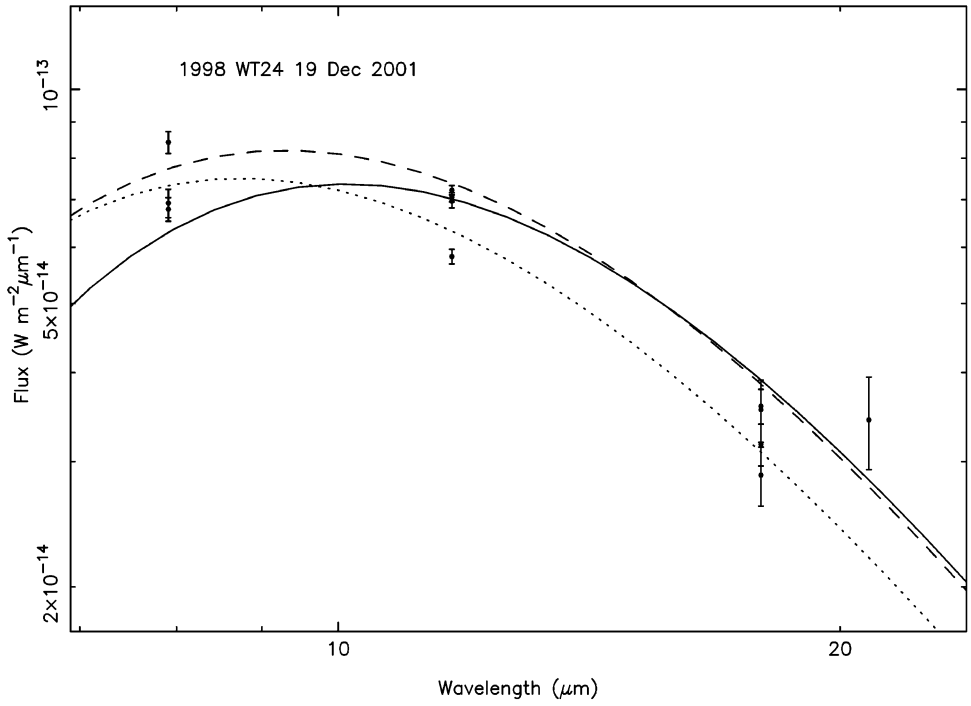

Figure 2

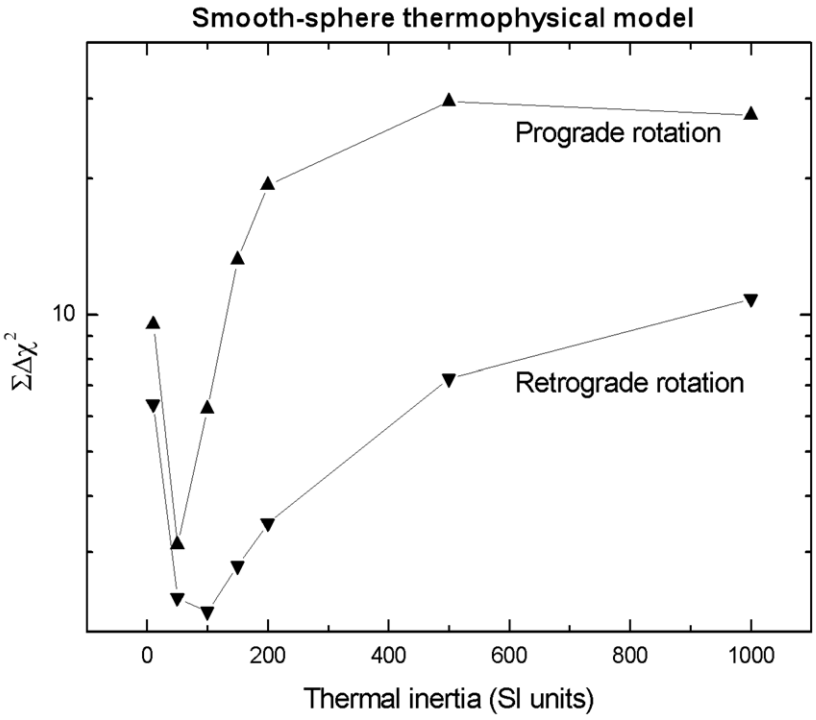

Figure 3

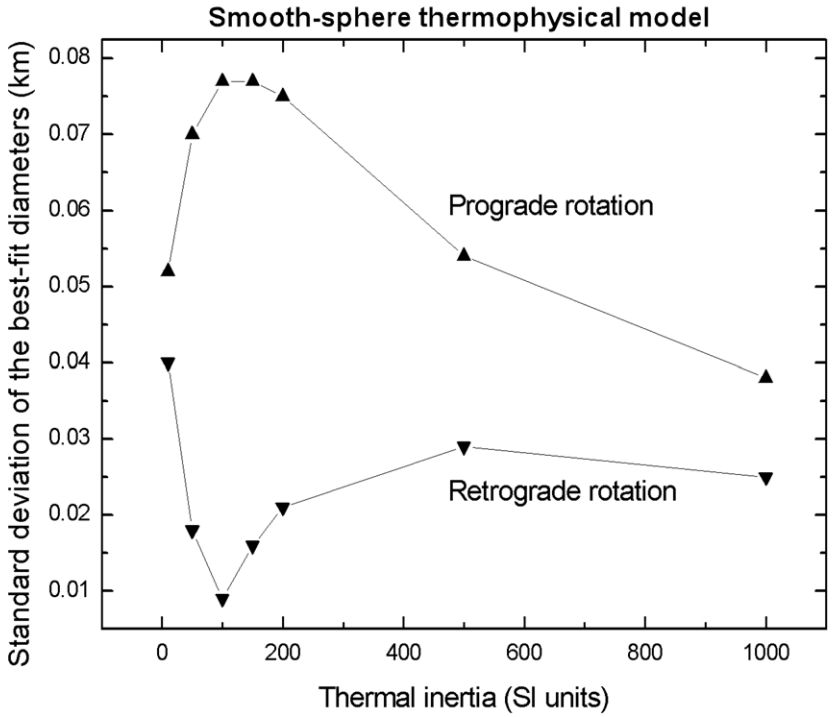

Figure 4

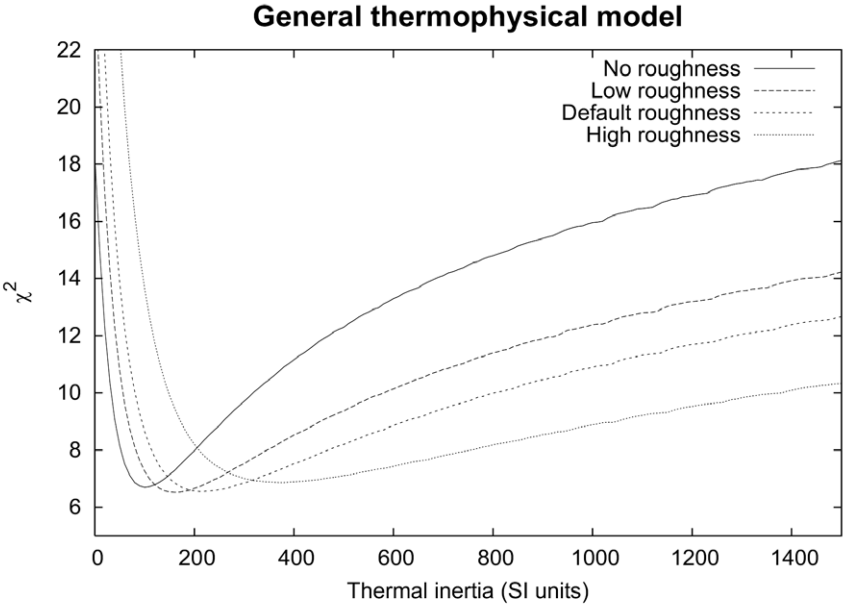

Figure 5